Applications of lattice-dynamic models to ^{67}Zn Lamb-Mössbauer factors and second-order Doppler shifts

M. Köfferlein, W. Potzel, M. Steiner, H. Karzel, W. Schiessl, and G. M. Kalvius
Physik Department E15, Technische Universität München, D-85747 Garching, Germany
(Received 6 March 1995; revised manuscript received 19 May 1995)

Using various lattice-dynamic models available in the literature we have calculated the Lamb-Mössbauer factor (LMF) and the second-order Doppler shift for the ^{67}Zn resonance in Zn metal, β' brass, ZnF_2, and the chalcogenides ZnO, ZnS, ZnSe, and ZnTe. Agreement with experimental results is satisfactory, in particular when lattice-dynamic models are used which include a good representation of eigenvectors. The large anisotropy of the LMF in Zn metal and in ZnF_2 is well reproduced. The shortcomings of the Debye approximation are pronounced even for systems with high symmetry.

I. INTRODUCTION

The 93.31-keV Mössbauer transition in ^{67}Zn offers remarkably high resolution for the determination of small changes in γ-ray energy.[1–3] Using ZnO single crystals and enriched ^{67}ZnO powder a relative energy resolution of 1.3×10^{-18} has been achieved.[4] This exceptionally high sensitivity has been used in gravitational redshift experiments[5] and for precision measurements of nuclear quadrupole interactions.[1,2] In addition, it has been demonstrated that this resonance is also a highly powerful tool for investigating lattice-dynamic properties, the Lamb-Mössbauer factor (LMF), and the second-order Doppler shift (SOD).[6–10] In Zn metal, for example, the LMF was found to be highly anisotropic: the ratio $(f_\perp/f_\parallel)$ of the LMF's perpendicular and parallel to the crystallographic c axis is ≈25 at 4.2 K and rises to ≈2000 at 47 K.[11] Furthermore, at 4.2 K and high external pressures (≈6.5 GPa) an electronic topological transition is observed where the LMF averaged over all directions in space abruptly drops by a factor of 2.[12]

The second-order Doppler shift S_{SOD} is difficult to determine experimentally. It is only one contribution to the experimentally observed center shift $S_C=S+S_{SOD}$ where the isomer shift S is determined by the s-electron density $\rho(0)$ at the nucleus. With most Mössbauer transitions, S_{SOD} is rather small and completely overwhelmed by S. In ^{67}Zn, however, S and S_{SOD} can be of the same magnitude. To investigate S_{SOD} it is essential to derive S separately, usually by theoretical calculations or vice versa, S_{SOD} has to be known to study changes of S.

In recent years various theoretical *ab initio* methods have been developed to calculate hyperfine interactions in solids.[13–15] The electric-field gradient can successfully be described even in systems with more complex crystallographic structures like the high-temperature superconductors.[16,17] The theoretical calculations of changes in $\rho(0)$, however, turn out to be much more demanding on the accuracy of the theoretical procedure because most often these changes are very small, typically 1 part in 20 000 or even less.

Theoretical calculations of $\rho(0)$ have been available for the zinc chalcogenides and for ZnF_2.[13,14,18] Together with the experimentally determined center shift S_C the results of these calculations can be used to predict S_{SOD}. Although lattice-dynamic models have been available in the literature for quite some time, these models have hardly been employed for calculations of LMF and SOD. In contrast to other more common lattice-dynamic properties like the specific heat, the LMF as well as the SOD are sensitive to the distribution of the kinetic energy among the various chemical constituents of the crystal. Therefore, for a detailed calculation of the LMF and SOD it is not sufficient to know the frequency distribution and dispersion relations. The eigenvectors or polarization vectors of the phonon modes are equally important in order to obtain reliable values for the LMF and SOD. The exceedingly high sensitivity of the ^{67}Zn resonance provides a stringent test for lattice-dynamic models. In this paper we report on our results of the direct calculation of S_{SOD} and the LMF for zinc systems from such models available in the literature.

II. PROCEDURE

A. General aspects

In the harmonic approximation, the equations of motion lead to an eigenvalue problem of the dynamical matrix $D_{\alpha\beta}\left(\begin{smallmatrix}\boldsymbol{q}\\ \kappa\kappa'\end{smallmatrix}\right)$,[19,20] which yields a relation between the eigenfrequencies $\omega_j(\boldsymbol{q})$ and the wave vector $\boldsymbol{q}$:

$$\sum_{\kappa'\beta}\left[D_{\alpha\beta}\begin{pmatrix}\boldsymbol{q}\\ \kappa\kappa'\end{pmatrix}-\omega_j^2(\boldsymbol{q})\,\delta_{\alpha\beta}\delta_{\kappa\kappa'}\right]e_\beta\begin{pmatrix}\kappa'\\ j\end{pmatrix}\boldsymbol{q}=0\ , \quad (1)$$

$$D_{\alpha\beta}\begin{pmatrix}\boldsymbol{q}\\ \kappa\kappa'\end{pmatrix}=\frac{1}{\sqrt{m_\kappa m_{\kappa'}}}\sum_{l'}\exp\left\{i\boldsymbol{q}\left[\boldsymbol{r}\begin{pmatrix}l'\\ \kappa'\end{pmatrix}-\boldsymbol{r}\begin{pmatrix}l\\ \kappa\end{pmatrix}\right]\right\}\Phi_{\alpha\beta}\begin{pmatrix}l & l'\\ \kappa & \kappa'\end{pmatrix}\ . \quad (2)$$

The primitive cells of the lattice are labeled by l and l', κ and κ' are the indices of the basis within the lattice cells l and l', respectively, and m_κ is the mass of the basis atom κ. $\Phi_{\alpha\beta}\left(\begin{smallmatrix}l & l'\\ \kappa & \kappa'\end{smallmatrix}\right)$ are the general second-order expansion coefficients of the potential energy, usually referred to as the *force constants*. The polarization vectors $\boldsymbol{e}(\kappa|_j^{\boldsymbol{q}})$ describe the direc-

tion of motion of the basis atom κ in the mode $(\boldsymbol{q},j)$ associated with frequency $\omega_j(\boldsymbol{q})$. For further details we refer to Ref. 21.

The Lamb-Mössbauer factor $f_{\boldsymbol{k}}$ can be written[22]

$$f_{\boldsymbol{k}}=\exp(-k^2\langle x^2\rangle_{\boldsymbol{k}}) , \tag{3}$$

where $\boldsymbol{k}$ is the photon wave vector, $\langle x^2\rangle_{\boldsymbol{k}}$ is the mean-square vibrational displacement of the Mössbauer nucleus in direction of the wave vector $\boldsymbol{k}$.

Expressing the mean-square displacement by phonon generation and destruction operators leads to the quantum-mechanical expression for the LMF,[23]

$$f_{\boldsymbol{k}}=\exp\left[-\frac{\hbar}{m_\kappa N}\sum_{j\boldsymbol{q}}\frac{\left|\boldsymbol{k}\cdot\boldsymbol{e}\left(\kappa\middle|\begin{matrix}\boldsymbol{q}\\ j\end{matrix}\right)\right|^2}{\omega_j(\boldsymbol{q})}\left(n_j(\boldsymbol{q},T)+\frac{1}{2}\right)\right] , \tag{4}$$

where κ labels the site of the Mössbauer nucleus, N is the number of unit cells of the finite crystal and

$$n_j(\boldsymbol{q},T)=\left[\exp\left(\frac{\hbar\omega_j(\boldsymbol{q})}{k_BT}\right)-1\right]^{-1}$$

is the occupation number of the phonon mode $(\boldsymbol{q},j)$ at temperature T. Because of the term $|\boldsymbol{k}\cdot\boldsymbol{e}(\kappa|^{\boldsymbol{q}}_j)|^2$ in Eq. (4) the LMF usually is anisotropic in systems of less than cubic symmetry. Only in the case of monatomic systems with isotropic lattice-dynamic properties where $|\boldsymbol{k}\cdot\boldsymbol{e}(\kappa|^{\boldsymbol{q}}_j)|^2=k^2/3$, Eq. (4) can be reduced to the more familiar expression

$$f=\exp\left[-\frac{\hbar k^2}{3m_\kappa N}\int_0^{\omega_{\max}}d\omega\,\frac{Z(\omega)}{\omega}\left(n(\omega,T)+\frac{1}{2}\right)\right] \tag{5}$$

with $\omega_{\max}$ and $Z(\omega)$ being the maximal phonon frequency and phonon frequency distribution, respectively.[21]

The second-order Doppler shift S_{SOD} is given in velocity units:[24]

$$S_{\mathrm{SOD}}=-\frac{1}{2c}\langle v^2\rangle , \tag{6}$$

where $\langle v^2\rangle$ is the mean-square velocity of the Mössbauer atom. The quantum-mechanical expression then becomes[25]

$$S_{\mathrm{SOD}}=-\frac{\hbar}{2m_\kappa cN}\sum_{j\boldsymbol{q}}\omega_j(\boldsymbol{q})\cdot\left|\boldsymbol{e}\left(\kappa\middle|\begin{matrix}\boldsymbol{q}\\ j\end{matrix}\right)\right|^2\left(n_j(\boldsymbol{q},T)+\frac{1}{2}\right) . \tag{7}$$

Again, only in the special case of monatomic systems where

$$\sum_\alpha\left|e_\alpha\left(\kappa\middle|\begin{matrix}\boldsymbol{q}\\ j\end{matrix}\right)\right|^2=\sum_{\kappa\alpha}\left|e_\alpha\left(\kappa\middle|\begin{matrix}\boldsymbol{q}\\ j\end{matrix}\right)\right|^2=1 ,$$

Eq. (7) can be expressed by

$$S_{\mathrm{SOD}}=-\frac{\hbar}{2m_\kappa cN}\int_0^{\omega_{\max}}d\omega\;\omega Z(\omega)\left(n(\omega,T)+\frac{1}{2}\right) . \tag{8}$$

In general, however, the eigenvectors $\boldsymbol{e}(\kappa|^{\boldsymbol{q}}_j)$ play a significant role for both LMF and SOD, and their knowledge is crucial for reliable numerical calculations. When employing rather simple lattice-dynamic models like the Debye model, this fact is not taken into account. For monatomic and isotropic systems such simple models may be sufficient.

B. Lattice-dynamic models

To calculate $f_{\boldsymbol{k}}$ and S_{SOD} numerically according to the equations given in Sec. I the force constants $\Phi_{\alpha\beta}(\begin{smallmatrix}l & l'\\ \kappa & \kappa'\end{smallmatrix})$ have to be obtained from lattice-dynamic models. A considerable number of models has been available in the literature. Most of them have been developed to provide a theoretical fit to experimental phonon-dispersion relations. For our investigations we have selected three models. They are preferred because of their widespread use and relative simplicity. One of them is suitable for metals, two have been extended to ionic systems which are partially covalent.

Within the *force constant model* or *Born-von Kármán model* all force constants are treated as independent parameters.[26] To simplify the model, interactions extending past a specific cutoff length are neglected. Such an approach may be sufficient for metals where the long-range Coulomb interaction can be expected to be effectively screened by conduction electrons. To reduce the relatively large number of independent force constants often an axially symmetric interaction between nearest neighbors is assumed (axially symmetric model).

The *rigid-ion model* (RIM) describes the interaction between two ions in the crystal by two contributions:[26] a short-range interaction due to the covalent bonding and repulsive overlap forces and a long-range interaction due to the Coulomb forces between the ions. The short-range interaction usually extends to the next- and second-nearest neighbors. For the Coulomb interaction the ions are assumed to be point charges with no internal structure, i.e., "rigid ions." The long-range Coulomb interaction leads to a more detailed description of the physical properties of the crystal and gives rise to a splitting of the optical-phonon branches at the Γ point.

The basic assumptions of the *shell model*[27–29] (SM) are the same as in the RIM, except that the point charges of the ions are replaced by polarizable ions consisting of a spherical massless shell and a heavy core. Both shell and core are charged and the intraionic shell-core interaction is described by an isotropic harmonic force. In addition, shell and core interact with the shells and cores of neighboring ions via Coulomb interaction and short-range interactions. The dynamical matrix consists of that of the RIM and an additional term which arises from the induced dipolar forces. In the simplest version of the SM the short-range interaction is assumed to be mediated only by the shells and, furthermore, the polarizability of the small cations is neglected. However, even the extended versions of the shell model often require effective *positive* electronic shell charges to satisfactorily reproduce experimental phonon-dispersion relations.

The *overlap shell model*[30] (OSM) is based on the SM but takes an additional contribution to the dynamical matrix due to "overlap polarization" into account. When the overlap of two neighboring electronic shells is enhanced due to the displacements of the ions, electronic charge is repelled from the regions of increased overlap. The redistribution of electronic charge contributes to the polarization of the ions. This so-called overlap polarization sometimes shows up as effective

positive shell charges within the SM. Although the equations of motion within the OSM are the same as within the SM, the overlap polarization gives a physically satisfying explanation of the effective positive shell charges.

Within the so-called *valence force field model* (VFFM) the interaction potential is expressed as a function of bond angles, leading to bond bending forces, and of bond lengths, giving rise to bond-stretching forces.[19,31,32] This model does not contain any long-range Coulomb interactions and is therefore well suited to describe the lattice dynamics of crystals with predominantly covalent bonding and of metals which are characterized by effectively screened ionic charges. In particular in combination with other lattice-dynamic models, the VFFM is a highly successful approximation to describe the short-range interaction due to partially covalent bonding.

The parameters of these phenomenological models have to be determined empirically. This is usually accomplished by fitting the calculated phonon-dispersion relations to inelastic neutron-scattering data, symmetry-point frequencies determined by first- or second-order Raman scattering or macroscopic quantities as elastic constants, and, in the case of the shell model, the dielectric constant in the limits of zero and infinite frequencies. Unfortunately, these quantities are not sensitive to the eigenvectors of the dynamic matrix but only to the frequency spectrum, thus allowing only the determination of the eigenvalues of the dynamic matrix.[33,34] The eigenvectors can only be derived if additional experimental data like neutron-scattering cross sections are available. As already mentioned, the calculation of LMF and SOD from the lattice-dynamic models described above requires the knowledge of the eigenvectors as well as of the frequency spectrum.

C. Details of calculation

Concerning the numerical procedure, in a first step, the force constants are calculated from the model parameters. Then the dynamical matrix is calculated and the resulting eigenvalue problem solved at each point of a dense $\boldsymbol{q}$ mesh in the irreducible Brillouin zone.[20] The $\boldsymbol{q}$ points are located on straight lines ("rays") from the center to the boundary of the Brillouin zone. The LMF is sensitive to low-frequency phonon modes. For this reason we did not distribute the $\boldsymbol{q}$ points on these rays uniformly but rather chose a smaller spacing in the central region of the Brillouin zone. Thus we were able to increase numerical accuracy considerably. The contribution of short-range interactions to the dynamical matrix is calculated via Eq. (2) directly from the force constants. In this respect the $\boldsymbol{q}$ mesh described above offers also a calculational advantage: the contribution of short-range interactions to the dynamical matrix decomposes into a product of two sums, one of them depending solely on the direction and the other solely on the magnitude of $\boldsymbol{q}$. Thus the direction-dependent sum has to be computed only once for each ray. To determine the dynamic matrix of the long-range Coulomb interaction we used the Ewald method.[19,20] This method decomposes the Coulomb matrix into two rapidly converging sums, one involving a summation over the direct lattice and the other a summation over the reciprocal lattice. For further details and explicit expressions for the two sums we refer to Ref. 19.

TABLE I. Experimental data for zinc metal compared to the numerical results obtained from the model of Ref. 36 using $m_{Zn}=67$. $f_\perp$ and $f_\parallel$ denote the LMF perpendicular and parallel to the c axis, respectively. ΔS_C and ΔS_{SOD} are the measured center shift and the calculated SOD relative to 4.2 K. The absolute SOD was calculated to be -53.08 μm/s at 4.2 K.

	Experimental	(Refs. 6, 35)	Theoretical	(Ref. 36)
T (K)	$f_\perp$ (%)	$f_\parallel$ (%)	$f_\perp$ (%)	$f_\parallel$ (%)
4.2	$1.07(^{+0.13}_{-0.12})$	$0.043(^{+0.088}_{-0.030})$	1.19	0.032
20.8	$0.80(^{+0.18}_{-0.15})$	$0.098(^{+0.53}_{-0.080})$	1.08	0.022
47	$0.40(^{+0.10}_{-0.05})$	$0.000\,18(^{+0.0067}_{-0.000\,17})$	0.62	0.0016
T (K)	$-\Delta S_C$ (μm/s)		$-\Delta S_{SOD}$ (μm/s)	
4.2	0.0		0.0	
20.8	0.37(8)		0.267	
47	4.46(19)		4.38	

We have investigated the following systems: zinc metal, β' brass, ZnF_2, ZnO, ZnS, ZnSe, and ZnTe. For all cases we have first calculated the dispersion relations to check for correct implementation of a particular model against published data. The LMF and SOD were obtained from Eqs. (4) and (7).

To assure good convergence, we used relatively dense $\boldsymbol{q}$ meshes, especially in cases of rather complex crystal structures. For ZnF_2, for example, a very dense $\boldsymbol{q}$ mesh with 23 900 points in the irreducible Brillouin zone was chosen. Such a dense $\boldsymbol{q}$ mesh proved to be necessary since ZnF_2 crystallizes with tetragonal rutile structure with two molecules within the unit cell. To test for convergence we calculated the lattice-dynamic parameters also with a drastically reduced $\boldsymbol{q}$ mesh of 8040 points. We found that f_x and f_z changed only by about 2×10^{-3} and f_y stayed practically constant.

For all zinc chalcogenides which crystallize either in the wurtzite or in the sphalerite structure, we chose a $\boldsymbol{q}$ mesh with 3680 points in the irreducible Brillouin zone. For ZnO with a hypothetical sphalerite structure (see Sec. III D), the LMF and the magnitude of S_{SOD} increased by only 1.6×10^{-3} and 2.0×10^{-3}, respectively, when the number of points was raised to 24 600, indicating again good convergence. The same situation holds for all other zinc chalcogenides investigated. For zinc metal which crystallizes in hcp structure and β' brass (ordered CsCl structure), $\boldsymbol{q}$ meshes with 2880, respectively, 2240 points were sufficient to obtain good numerical accuracy.

III. RESULTS AND DISCUSSION

A. Zinc metal

Zinc metal which crystallizes in hexagonal close-packed structure with an unusually large c/a ratio ($c/a=1.86$) provides a stringent test for lattice-dynamical calculations because of the pronounced anisotropy of many physical properties including the LMF. In Table I experimental data[35] on LMF and SOD at various temperatures are compared with our calculations using the lattice-dynamic model of Refs. 36

TABLE II. Experimental data for β' brass compared to the numerical results obtained from the force constant model of Ref. 39 using $m_{Zn}=67$ and from the corresponding phonon density of states $Z(\omega)$ (Ref. 7). In the latter case the influence of the eigenvectors is neglected. f denotes the LMF. ΔS_C and ΔS_{SOD} are the measured center shift and the calculated SOD relative to 4.2 K. The absolute SOD was calculated to be -64.34 μm/s at 4.2 K and -63.51 μm/s at 4.2 K from the force constant model and the phonon density of states, respectively.

	Experimental (Ref. 7)	Theoretical (Ref. 39)	Theoretical from $Z(\omega)$ (Ref. 7)
T (K)	f (%)	f (%)	f (%)
4.2	0.80(14)	0.95	0.85
20	0.67(10)	0.80	0.74
40	0.34(6)	0.43	0.42
55	0.12(3)	0.21	0.21
60	0.11(3)	0.17	0.17
T (K)	$-\Delta S_C$ (μm/s)	$-\Delta S_{SOD}$ (μm/s)	$-\Delta S_{SOD}$ (μm/s)
4.2	0.0	0.0	0.0
20	0.128(48)	0.148	0.149
40	1.887(59)	1.77	1.85
55	4.98(13)	4.58	4.80
60	5.91(14)	5.82	6.09

and 37. This modified axially symmetric (MAS) model is an extension of the axially symmetric VFFM proposed by DeWames.[36] The pronounced lattice-dynamic anisotropy in zinc metal is taken into account by different bond-stretching forces perpendicular and parallel to the crystallographic c axis. The corresponding force constants were obtained from a fit of the model to experimental dispersion relations. The interactions extend to the sixth-nearest neighbors. References 36 and 37 also aimed at the calculation of LMF and SOD, thus providing a test for our calculation procedure. The MAS model is able to reproduce our experimental data, in particular the large anisotropy of the LMF, very well. At 4.2 K, the LMF parallel to the c axis ($f_\parallel$) is ≈ 25 times smaller than perpendicular ($f_\perp$) to it. For this reason the experimental derivation of $f_\parallel$ is a difficult problem which is reflected in the relatively large error bars for $f_\parallel$.

The measured change (ΔS_C) of the center shift and the calculated variation (ΔS_{SOD}) of the second-order Doppler shift with temperature are in good agreement. This strongly confirms our earlier conclusion[11] that there is no explicit temperature dependence of the isomer shift (S) up to ≈ 50 K.

B. β' brass

The alloy $Cu_{0.5}Zn_{0.5}$ (β' brass) forms an ordered CsCl structure below 725 K where each Zn atom is surrounded by eight Cu atoms and vice versa. Also this system has been investigated earlier by ^{67}Zn-Mössbauer spectroscopy.[7,38] From point of view of lattice dynamics β' brass is an interesting case because of its cubic structure, the similar masses of Cu and Zn, and similar binding forces between them.[7] The kinetic energy, e.g., is expected to be shared almost equally between both constituents. Since eigenvectors are not important, it should be possible to obtain LMF and SOD directly from the phonon frequency distribution $Z(\omega)$ in analogy to monatomic isotropic systems. The phonon density of states is introduced into Eqs. (4) and (7) by setting $\Sigma_\alpha |e_\alpha(\kappa|_j^q)|^2 = 1/2$ and $\Sigma_\alpha |k_\alpha \cdot e_\alpha(\kappa|_j^q)|^2 = k^2/6$ for two-atomic, cubic compounds and employing the definition of the phonon density of states. For comparison, we have also used a detailed Born-von Kármán model[39] with eight adjustable parameters for our numerical calculations. For a good description of the experimental phonon-dispersion relations force constants out to the fourth-nearest-neighbor shell are required. However, all tangential-type force constants except for the first-nearest neighbor shell have been neglected. As demonstrated by Table II, the experimental results are reproduced very well by the numerical calculations. Comparing the force constant model[39] with the density-of-states scheme we also find very good agreement. This justifies the use of the phonon density of states in cubic intermetallic compounds with similar constituents. A small discrepancy, however, remains due to the slightly different masses and force constants introduced by the model for the two constituents. The close agreement between the changes of the experimental center shift S_C and the calculated SOD clearly demonstrates that also for this alloy the explicit temperature dependence of the isomer shift is negligibly small within the temperature range investigated.

C. Zinc fluoride

ZnF_2 crystallizes with rutile-type structure with two ZnF_2 molecules in the tetragonal unit cell. Each Zn is surrounded by six F at the corners of a distorted octahedron. Several physical properties show anisotropic behavior, e.g., the axial compressibilities, the coefficients of thermal expansion at low temperatures, and the LFM. We have performed lattice-dynamic calculations using a shell-model description.[40] In addition, in Ref. 40 short-range interactions due to the partially covalent bonding are taken into account

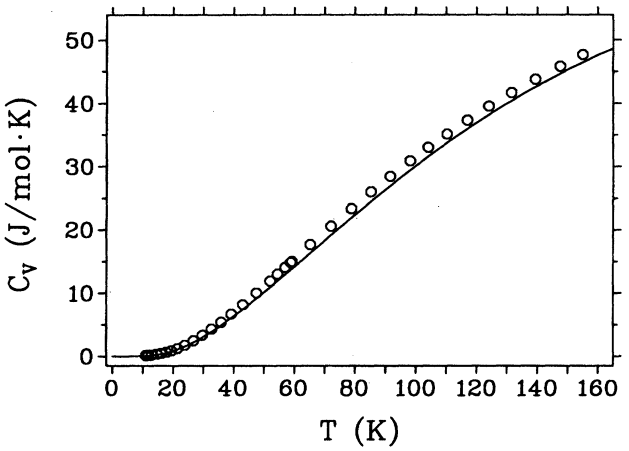

FIG. 1. Experimental specific-heat data (circles) for ZnF_2 compared to theoretical results (full line) obtained from the model of Ref. 40. The experimental values are taken from Ref. 55.

within a two-parameter VFFM which includes only bond-bending forces.[40] Contrary to simpler continuum models discussed in the literature[8,41] this "expanded" shell model is able to describe the specific-heat data of ZnF_2 quite well as shown in Fig. 1. There is a slight tendency to smaller values compared to the experimental data, in particular at temperatures above $\approx$40 K. Still, we are convinced that this model is by far the best which is available at present. It also reproduces the SOD as well as the pronounced anisotropy of the LMF. Simpler models[8,41] fail, essentially because they do not take into account optical-phonon modes which are already excited at temperatures of $\approx$30 K. Details concerning the ^{67}Zn-Mössbauer measurements and the results of our numerical calculations have recently been published[9] and will not be considered further in the present paper.

D. Zinc chalcogenides

1. Ambient pressure

The zinc chalcogenides ZnO, ZnS, ZnSe, and ZnTe are representatives of II-VI semiconductors which are expected to gain enormous technological importance due to applications in optical devices. The compounds crystallize in either the hexagonal wurtzite or the cubic zinc-blende phases, or both. Each cation is tetrahedrally coordinated by four anions, and vice versa. Such a coordination favors sp^3 bonding, the ionic part of the chemical bond, however, plays an important role, even in ZnTe. For this reason the shell model (SM) and the rigid-ion model (RIM) are well suited to describe the lattice dynamics in zinc chalcogenides. Table III gives a short characterization of all models used in the present investigation. Most models have been optimized to reproduce experimentally derived phonon frequencies and elastic constants. Unfortunately, these properties are not sensitive to the eigenvectors of the dynamical matrix. The overlap shell model (OSM) of Kunc and Bilz,[42] however, has successfully been extended to include nonlinear probabilities of the atoms to reproduce experimental cross sections of second-order Raman scattering. Since these cross sections depend on the eigenvectors this model is expected to provide also a good eigenvector representation.

TABLE III. Compilation of models employed with the zinc chalcogenides. nP denotes the number of parameters, VFFM is the valence force field parametrization scheme, RIM and SM are the rigid-ion model and the shell model, respectively. OSM is the overlap shell model, an extended version of the SM (Ref. 30). ZnO which crystallizes in the wurtzite structure is in some models approximated by sphalerite (ZnS) structure, as for example in Ref. 42. Where a single reference contains different alternative parameter sets, the model is further specified by Roman numbers in parentheses.

Compound	Description	Reference
ZnO	10*P* VFFM+OSM Sphalerite	42
	10*P* VFFM+SM Wurtzite	46
ZnS	10*P* VFFM+OSM	42
	11*P* RIM	47
	10*P* VFFM+SM	54 (I)
	10*P* VFFM+SM	54 (Ia)
	10*P* VFFM+SM	54 (II)
	10*P* VFFM+SM	31
	6*P* VFFM+RIM	31
ZnSe	10*P* VFFM+OSM	42
	7*P* RIM	45
	11*P* RIM	43
	11*P* RIM	47
	7*P* RIM	44
ZnTe	10*P* VFFM+OSM	42
	10*P* VFFM+SM	54 (I)
	10*P* VFFM+SM	54 (Ia)
	7*P* RIM	44

All models investigated give a good description of available data on bulk properties, like the specific heat. As an example, Fig. 2 shows experimental specific-heat data in comparison with theoretical results obtained from the combination of OSM and VFFM.[42] A similarly close agreement was found for the other models. However, as can be noticed from Table IV the variation is much larger for the Mössbauer parameters LMF and SOD. As mentioned earlier this can mainly be attributed to the different eigenvector representations. From a comparison of the LMF values we have to abandon several of the parameter sets. For ZnSe, e.g., the models of Refs. 43, 44, and 45 can be ruled out.

For ZnO, the model of Ref. 46 is of particular interest. Since it is tailored to the hexagonal (wurtzite) structure, it allows the investigation of anisotropic effects. Table V shows that, in agreement with experiment, the anisotropy of the LMF is rather small. The model of Ref. 42 which has been designed for a hypothetical zinc-blende structure gives an isotropic (average) value for the LMF. Both models reproduce the experimental data on the LMF and the SOD, including their temperature dependences, very well.

The model of Kunc and Bilz[42] provides a good systematic description of the LMF and the SOD for all zinc chalcogenides. We have used this model to calculate the second-order Doppler shift S_{SOD} for these systems. From the experimentally known center shift S_C we can then derive the

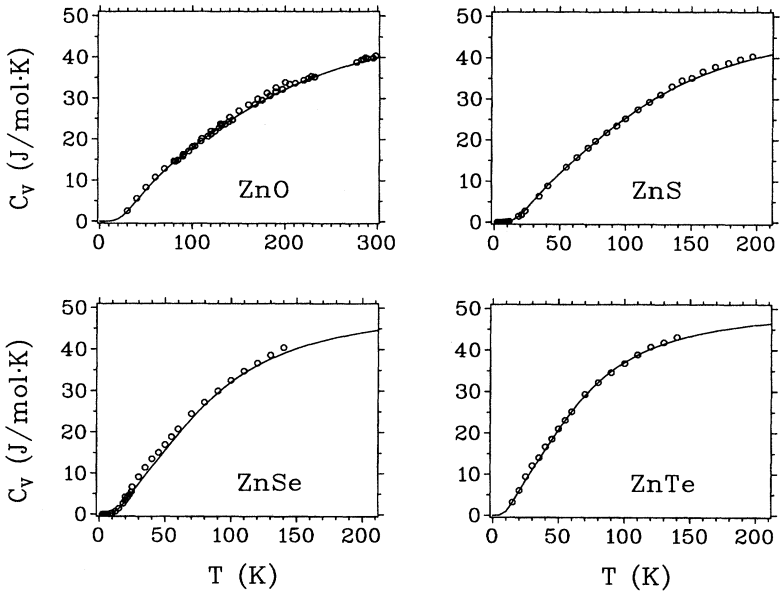

FIG. 2. Experimental specific-heat data (circles) for zinc chalcogenides compared to theoretical results (full line) obtained from the model of Ref. 42. The experimental values are taken from Ref. 56 for ZnO, Refs. 57 and 58 for ZnS, Refs. 57 and 44 for ZnSe, and Ref. 44 for ZnTe.

isomer shift S which itself is determined by the s electron density $\rho(0)$ at the ^{67}Zn nucleus. As described in more detail in Refs. 13, 14, and 35 this procedure fits very well to theoretical results for $\rho(0)$ obtained from *ab initio* Hartree-Fock cluster calculations.

2. High external pressure

The pressure dependence of lattice-dynamic parameters is a consequence of anharmonic properties of the lattice. In quasiharmonic approximation this pressure dependence is described by assuming a harmonic potential at each pressure but allowing the force constants to be pressure dependent. Only few models have been published so far which are optimized for pressure-dependent lattice-dynamic effects. For zinc chalcogenides the model of Talwar *et al.*[47] is available which describes the pressure dependence of force constants for ZnS, ZnSe, and ZnTe. It is a rigid-ion model with 11 independent parameters (RIM11) which have been optimized

TABLE IV. Experimental data obtained for the zinc chalcogenides at 4.2 K compared to theoretical results using $m_{Zn}=67$. f denotes the LMF, S_{SOD} the absolute SOD. In the case of ZnO, where a weak anisotropy is present, average values for the LMF are given. ΔS_{SOD} denotes the SOD relative to the result for ZnO calculated from the model of Ref. 42.

System	Experimental (Ref. 35)	Theoretical			Reference
	f (%)	f (%)	$-S_{SOD}$ (μm/s)	ΔS_{SOD} (μm/s)	
ZnO	2.0(1)	1.94	79.67	0.0	42
		2.28	86.13	−6.46	46
ZnS	0.74(5)	0.670	65.07	14.60	42
		0.511	60.45	19.22	47
		0.878	69.86	9.81	54 I
		0.439	67.74	11.93	54 Ia
		0.672	66.50	13.17	54 II
		0.781	69.61	10.06	31 SM
		0.689	62.06	17.61	31 RIM
ZnSe	0.50(6)	0.626	66.43	13.24	42
		0.949	75.69	3.98	45
		1.20	76.05	3.62	43
		0.420	61.19	18.48	47
		1.85	79.50	0.17	44
ZnTe	0.30(5)	0.241	57.52	22.15	42
		0.351	60.73	18.94	54 I
		0.429	61.91	17.76	54 Ia
		0.300	56.10	23.57	44

TABLE V. Experimental data for ZnO at various temperatures compared to theoretical results using $m_{Zn}=67$. $f_\perp$ and $f_\parallel$ denote the LMF perpendicular and parallel to the crystallographic c axis, respectively, ΔS_{SOD} is the SOD relative to 4.2 K. The model of Ref. 42 is designed for the hypothetical sphalerite structure and thus is intrinsically isotropic; therefore f denotes the average LMF.

	Experimental (Ref. 53)		Theoretical (Ref. 46)		Theoretical (Ref. 42)
T (K)	$f_\perp$ (%)	$f_\parallel$ (%)	$f_\perp$ (%)	$f_\parallel$ (%)	f (%)
4.2	2.06(21)	2.03(12)	2.34	2.28	1.94
19.4			2.18	2.12	1.84
20.7		2.00(14)	2.16	2.10	1.83
40.8	1.42(15)	1.48(10)	1.62	1.58	1.41
56.2	1.24(13)	0.80(6)	1.12	1.09	0.98
77.3	0.64(7)	0.44(3)	0.58	0.57	0.51
T (K)	$-\Delta S_C$ (μm/s)		$-\Delta S_{SOD}$ (μm/s)		$-\Delta S_{SOD}$ (μm/s)
4.2	0.0		0.0		0.0
19.4	0.080(3)		0.051		0.045
20.7	0.08(3)		0.068		0.062
40.8	1.50(3)		1.16		1.30
56.2	4.22(4)		3.45		3.85
77.3	9.01(3)		8.55		9.36

for pressure-dependent Raman-scattering data. Unfortunately, such data are only available at ambient pressure and close to the structural phase transition at ≈ 13.7 GPa.[48] For pressures within this region the model parameters were linearly interpolated.[47] Figure 3 shows a comparison between our experimental and theoretical results for the Lamb-Mössbauer factor of ZnSe.[49] The agreement at ambient pressure is very good. At elevated pressures, the experimental LMF increases at first and then drops when the volume reduction exceeds $\approx 8\%$. The RIM11, however, predicts a continuous decrease of the LMF. As has been discussed in more detail in Refs. 49 and 50 the decrease of the LMF with reduced volume is caused by the attractive short-range next-nearest-neighbor interaction. It decreases due to an increased screening of the Coulomb force between the zinc ions by bonding electrons. This leads to a reduction of the frequency of the transverse acoustic (TA) mode which is reflected in the decrease of the LMF.

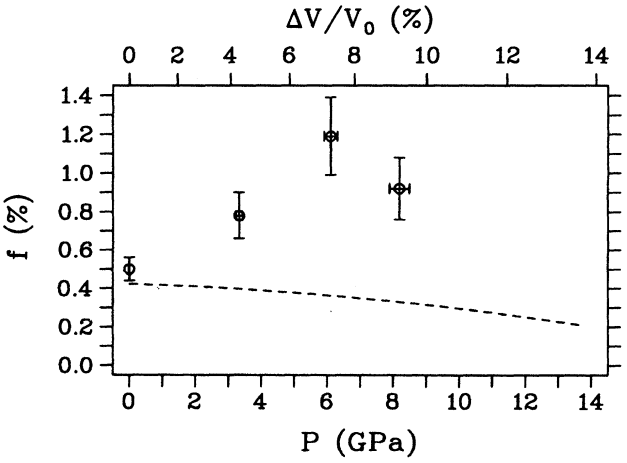

FIG. 3. Volume dependence of the LMF of ^{67}ZnSe. Dotted line: theoretical results (RIM11); circles: experimental data.

The discrepancy between the prediction of RIM11 and experimental results at high pressures is probably due to the linear interpolation of the model parameters mentioned above and shortcomings within the simple RIM itself. For a detailed description of the LMF more elaborate models are required. Still, for ZnSe RIM11 reproduces the LMF at ambient pressure quite well and shows how the crystallographic phase transition is already reflected in a softening of phonon modes much below the phase transformation.[49–51]

In addition, we have used RIM11 to calculate the pressure dependence of the second-order Doppler shift S_{SOD} in order to derive the isomer shift $S=S_C-S_{SOD}$ from the measured center shift S_C. We find a considerable rise of the s electron density $\rho(0)$ at the Zn nucleus with pressure due to a strong increase of covalency of the Zn-Se bond. Further details including the results of Hartree-Fock cluster calculations are given in Refs. 49 and 50.

E. Comparison with Debye model

One might argue that for systems with cubic symmetry and nearly equal masses of the constituents the Debye model can be expected to represent a good approximation to describe lattice-dynamic effects. In this respect β' brass and ZnSe are cases of particular interest. To answer this question we have calculated the moments $m(-1)$ and $m(+1)$ of the phonon density of states $Z(\omega)$. At low temperatures, these moments are proportional to the mean-square atomic displacements $\langle x^2\rangle$ and mean-square atomic velocities $\langle v^2\rangle$ which in turn determine the LMF and SOD, respectively. From an observed value for the LMF an effective Debye temperature θ_{LMF} can be derived assuming that the phonon

frequency distribution can be approximated by a Debye-type behavior. Similarly, from an observed value for the SOD, an effective Debye temperature θ_{SOD} can be obtained. If the Debye approximation holds, the ratio of the corresponding Debye temperatures $\theta_{SOD}/\theta_{LMF}$ should be equal to unity. This, however, is not what we find. For β' brass and ZnSe we obtain the values 1.07 and 1.20, respectively. The latter number is typical for other zinc chalcogenides as well: we derive 1.12 (ZnO), 1.16 (ZnS), and 1.24 (ZnTe). The main reason for $\theta_{SOD}/\theta_{LMF}$ being larger than unity can be attributed to an outstanding feature which is common to the frequency distributions of all zinc chalcogenides (and to a lesser extent also to the case of β' brass): optical branches exhibit pronounced peaks and they are well separated from the acoustic branches.[35] In the calculations of the LMF, these high-frequency phonons are less important, because $Z(\omega)$ is weighted by ω^{-1}. However, for the SOD the weighting factor is ω^{+1} and high-frequency phonons are essential. For ^{67}Zn-Mössbauer spectroscopy a difference in the Debye temperature of 20% (at $\theta=300$ K) would result in a change of SOD by ≈ 14 μm/s. This value, unfortunately, is comparable to typical isomer shifts between zinc chalcogenides.[13,35] Therefore, in almost all zinc systems investigated, the Debye model turns out to be too poor an approximation. We reach the same conclusion with respect to a satisfying description of the specific heat in these compounds.

For noncubic systems the Debye approximation may indeed fail completely. A case in point is zinc metal at high external pressures.[12,52] Within the Debye approximation the increase in LMF with pressure leads to a considerable rise in θ_{LMF}. If the same rise is assumed for θ_{SOD} a change of the SOD is predicted which is larger than the observed change of the center shift. Thus the s electron density $\rho(0)$ at the ^{67}Zn nucleus in zinc metal is expected to increase with pressure. Theoretical linearized augmented plane-wave calculations, however, show that $\rho(0)$ actually *decreases* when pressure is applied,[12] i.e., the Debye model seriously overestimates the change of the SOD.

IV. CONCLUSIONS

^{67}Zn-Mössbauer spectroscopy is a sensitive tool to investigate the mean-square atomic displacement and the mean-square atomic velocity of Zn atoms in solids and provides a basis for a stringent test of lattice-dynamic models. Using various force-constant models available in the literature we have calculated the LMF and the SOD for zinc metal, a Cu-Zn alloy, and several zinc compounds. Good agreement with experimental results can be reached if the models provide not only a detailed description of dispersion relations and phonon density of states but also a reasonable representation of eigenvectors. This has convincingly been demonstrated in particular for the anisotropic systems, Zn metal and ZnF_2. For all systems investigated, the Debye model is an insufficient approximation for a reliable derivation of the LMF and SOD even in cases of high symmetry. The cubic zinc chalcogenides (sphalerite structure) and β' brass (CsCl structure) are pertinent examples.

ACKNOWLEDGMENTS

We would like to gratefully acknowledge the continuous support and the excellent cooperation of the cyclotron group at the Forschungszentrum Karlsruhe, and would like to thank especially Dr. H. Schweickert, K. Assmus, and W. Maier. This work has been funded by the German Federal Minister for Research and Technology (BMFT) under Contract No. KA3TUM and the Forschungszentrum Karlsruhe.

[1] G. J. Perlow, W. Potzel, R. M. Kash, and H. de Waard, J. Phys. (Paris) Colloq. **35**, C6-197 (1974).
[2] W. Potzel, Th. Obenhuber, A. Forster, and G. M. Kalvius, Hyperfine Interact. **12**, 135 (1982).
[3] P. Helistö, E. Ikonen, T. Katila, W. Potzel, and K. Riski, Phys. Rev. B **30**, 2345 (1984).
[4] W. Potzel, Hyperfine Interact. **40**, 171 (1988).
[5] W. Potzel, C. Schäfer, M. Steiner, H. Karzel, W. Schiessl, M. Peter, G. M. Kalvius, T. Katila, E. Ikonen, P. Helistö, J. Hietaniemi, and K. Riski, Hyperfine Interact. **72**, 197 (1992).
[6] W. Potzel, W. Adlassnig, J. Moser, C. Schäfer, M. Steiner, and G. M. Kalvius, Phys. Rev. B **39**, 8236 (1989).
[7] M. Peter, W. Potzel, M. Steiner, C. Schäfer, H. Karzel, W. Schiessl, G. M. Kalvius, and U. Gonser, Phys. Rev. B **47**, 753 (1993).
[8] M. Steiner, W. Potzel, C. Schäfer, W. Adlassnig, M. Peter, H. Karzel, and G. M. Kalvius, Phys. Rev. B **41**, 1750 (1990).
[9] M. Steiner, W. Potzel, M. Köfferlein, H. Karzel, W. Schiessl, G. M. Kalvius, D. W. Mitchell, N. Sahoo, H. H. Klauss, T. P. Das, R. S. Feigelson, and G. Schmidt, Phys. Rev. B **50**, 13 355 (1994).
[10] M. Steiner, M. Köfferlein, W. Potzel, H. Karzel, W. Schiessl, G. M. Kalvius, D. W. Mitchell, N. Sahoo, H. H. Klauss, T. P. Das, R. S. Feigelson, and G. Schmidt, Hyperfine Interact. **93**, 1453 (1994).
[11] W. Potzel, W. Adlassnig, U. Närger, Th. Obenhuber, K. Riski, and G. M. Kalvius, Phys. Rev. B **30**, 4980 (1984).
[12] W. Potzel, M. Steiner, H. Karzel, W. Schiessl, M. Köfferlein, G. M. Kalvius, and P. Blaha, Phys. Rev. Lett. **74**, 1139 (1995).
[13] D. W. Mitchell, T. P. Das, W. Potzel, G. M. Kalvius, H. Karzel, W. Schiessl, M. Steiner, and M. Köfferlein, Phys. Rev. B **48**, 16 449 (1993).
[14] D. W. Mitchell, T. P. Das, W. Potzel, M. Köfferlein, H. Karzel, W. Schiessl, M. Steiner, and G. M. Kalvius, Hyperfine Interact. **90**, 411 (1994).
[15] P. Blaha, K. Schwarz, and P. H. Dederichs, Phys. Rev. B **37**, 2792 (1988).
[16] N. Sahoo, S. Markert, and T. P. Das, Phys. Rev. B **41**, 220 (1990).
[17] K. Schwarz, C. Ambrosch-Draxl, and P. Blaha, Phys. Rev. B **42**, 2051 (1990).
[18] P. Blaha (private communication).
[19] G. Venkataraman, L. A. Feldkamp, and V. C. Sahni, *Dynamics of Perfect Crystals* (MIT Press, Cambridge, 1975).
[20] M. Köfferlein, Diploma thesis, Technische Universität München,

D-85747 Garching, Germany, 1993.
[21] A. A. Maradudin, in *Dynamical Properties of Solids*, edited by G. K. Horton and A. A. Maradudin (North-Holland, Amsterdam, 1974), Vol. 1.
[22] H. Frauenfelder, *The Mössbauer Effect* (Benjamin, New York, 1962).
[23] P. Brüesch, in *Phonons: Theory and Experiments II*, edited by M. Cardona, P. Fulde, K. von Klitzing, and H.-J. Queisser, Springer Series in Solid State Sciences, Vol. 65 (Springer-Verlag, Heidelberg, 1986).
[24] B. D. Josephson, Phys. Rev. Lett. **4**, 341 (1960).
[25] R. M. Housley and F. Hess, Phys. Rev. **146**, 517 (1966).
[26] M. Born and K. Huang, *Dynamical Theory of Crystal Lattices*, 4th ed. (Oxford University Press, Oxford, 1966).
[27] W. Cochran, R. A. Cowley, G. Dolling, and M. M. Elcombe, Proc. R. Soc. London Ser. A **293**, 433 (1966).
[28] J. G. Traylor, H. G. Smith, R. M. Nicklow, and M. K. Wilkinson, Phys. Rev. B **3**, 3457 (1971).
[29] B. G. Dick and A. W. Overhauser, Phys. Rev. **112**, 90 (1958).
[30] H. Bilz, M. Buchanan, K. Fischer, R. Haberkorn, and U. Schröder, Solid State Commun. **16**, 1023 (1975).
[31] L. A. Feldkamp, D. K. Steinman, N. Vagelatos, J. S. King, and G. Venkataraman, J. Phys. Chem. Solids **32**, 1573 (1971).
[32] D. L. Price, J. M. Rowe, and R. M. Nicklow, Phys. Rev. B **3**, 1268 (1971).
[33] W. Cochran, Acta Crystallogr. A **27**, 556 (1971).
[34] R. S. Leigh, B. Szigeti, and V. K. Tewary, Proc. R. Soc. London Ser. A **320**, 505 (1971).
[35] W. Potzel, in *Mössbauer Spectroscopy Applied to Magnetism and Materials Science*, edited by G. J. Long and F. Grandjean (Plenum, New York, 1993), Vol. 1.
[36] R. E. DeWames, T. Wolfram, and G. W. Lehman, Phys. Rev. **138**, A717 (1965).
[37] W. T. Vetterling and D. Candela, Phys. Rev. B **27**, 5394 (1983).
[38] W. Adlassnig, W. Potzel, J. Moser, W. Schiessl, U. Potzel, C. Schäfer, M. Steiner, H. Karzel, M. Peter, and G. M. Kalvius, Phys. Rev. B **40**, 7469 (1989).
[39] G. Dolling and G. Gilat, in *Inelastic Scattering of Neutrons* (IAEA, Vienna, 1965), Vol. 1, p. 343.
[40] C. Benoit and J. Giordano, J. Phys. C **21**, 5209 (1988).
[41] S. P. Tewari and P. Silotia, Phys. Rev. B **45**, 7471 (1992).
[42] K. Kunc and H. Bilz, Solid State Commun. **19**, 1027 (1976).
[43] B. Hennion, F. Moussa, G. Pepy, and K. Kunc, Phys. Lett. **36A**, 376 (1971).
[44] J. C. Irwin and J. LaCombe, J. Appl. Phys. **45**, 567 (1974).
[45] D. N. Talwar and B. K. Agrawal, Solid State Commun. **11**, 1691 (1972).
[46] K. Thoma, B. Dorner, G. Duesing, and W. Wegener, Solid State Commun. **15**, 1111 (1974).
[47] D. N. Talwar, M. Vandevyver, K. Kunc, and M. Zigone, Phys. Rev. B **24**, 741 (1981).
[48] B. A. Weinstein, Solid State Commun. **24**, 595 (1977).
[49] M. Köfferlein, H. Karzel, W. Potzel, W. Schiessl, M. Steiner, G. M. Kalvius, D. W. Mitchell, and T. P. Das, Hyperfine Interact. **93**, 1505 (1994).
[50] H. Karzel, W. Potzel, M. Köfferlein, W. Schiessl, M. Steiner, U. Hiller, G. M. Kalvius, D. W. Mitchell, T. P. Das, P. Blaha, and M. P. Pasternak (unpublished).
[51] K. Kunc and R. M. Martin, in *Ab Initio Calculation of Phonon Spectra*, edited by J. T. Devreese, V. E. Van Doren, and P. E. Van Camp (Plenum, New York, 1983), p. 65.
[52] M. Steiner, W. Potzel, H. Karzel, W. Schiessl, M. Köfferlein, G. M. Kalvius, and P. Blaha (unpublished).
[53] C. Schäfer, W. Potzel, W. Adlassnig, P. Pöttig, E. Ikonen, and G. M. Kalvius, Phys. Rev. B **37**, 7247 (1988).
[54] N. Vagelatos, D. Wehe, and J. S. King, J. Chem. Phys. **60**, 3613 (1974).
[55] J. W. Stout and E. Catalano, J. Chem. Phys. **23**, 2013 (1955).
[56] *Thermophysical Properties of Matter*, edited by Y. S. Touloukian and E. H. Buyco (IFI/Plenum, New York, 1970), Vol. 5.
[57] J. A. Birch, J. Phys. C **8**, 2043 (1975).
[58] K. Clusius and P. Harteck, Z. Phys. Chem. **134**, 243 (1928).